Deep Learning-Based Eye Tracking Analysis for Autism Spectrum Disorder Report

Callyn Villanueva, Christian Oliveto

Abstract

Eye tracking technology has shown promise in aiding the diagnosis of autism spectrum disorder (ASD) by capturing atypical gaze patterns in individuals with ASD. This project aims to develop a deep learning-based system for analyzing eye tracking data to assist in the early diagnosis of ASD. The system will be trained on a dataset of eye tracking recordings from individuals with and without ASD to learn patterns associated with ASD-related gaze behaviors. The project will focus on developing a deep learning model for accurately classifying selected eye tracking data as belonging to individuals with ASD or typical development. We are also interested in identifying any trends in the data.

1 Background

Children with Autism Spectrum Disorder (ASD) exhibit distinct patterns of gaze behavior that have been a subject of extensive research. Some studies suggest that these children demonstrate normal patterns of cueing, indicating an awareness of the significance of eye contact. However, other studies reveal atypical gaze behaviors, highlighting the complexity of understanding social communication in ASD. The prevalence of ASD has steadily increased, with current estimates indicating that 1 in 44 children in the United States meet criteria for this disorder. Diagnosis and symptomatology of ASD vary among healthcare professionals, and the nature of symptoms has evolved over time. Understanding gaze behavior in children with ASD is crucial for developing effective interventions and improving their social interactions and communication skills. [1][2] Understanding the short- and long-term effects of atypical

gaze behavior in individuals with ASD underscores the significance of studying this unique behavior in the everyday environments they encounter. Eye tracking technology has played a pivotal role in these studies, enabling researchers to elucidate intriguing findings that could potentially broaden the diagnostic criteria for autism and deepen our understanding of this developmental disorder.

In a pioneering study, Noris et al. (2011) examined the gaze behavior of children aged 3-9 with ASD during a dyadic interaction in a natural setting. Participants wore a head-mounted 'WearCam' to record their field of view and gaze direction. The interaction involved blowing soap bubbles, playing with a mechanical toy, a toy car, and a small ball provided by the experimenter. The study found that compared to typically developing (TD) controls, children with ASD exhibited more downward looks and explored their lateral field of view more extensively. This behavior was attributed to the downcast gaze phenomenon in autism, which is believed to be a response to sensory overload and hypersensitivity to visual stimuli in real-life environments.

Fixation abnormalities measured by eye tracking have been associated with children with autism spectrum disorder (ASD), yet the underlying dynamics of fixation patterns across different ages remain unclear along with other aspects of eye behavior such as pupil dilation.

The study by Camero et al. shared a similar goal to ours, aiming to investigate whether measurements of gaze following and pupillary dilation during a linguistic interaction task could serve as potential objective biomarkers for early ASD diagnosis [3]. The experiment involved 20 children aged between 17 and 24 months, comprising 10 neurotypical children (NT) and 10 children with a higher likelihood of developing ASD. During the experiment, a human face was displayed on a monitor, pronouncing pseudowords associated with pseudo-objects. Gaze following and pupil dilation were recorded using eye-tracking technology. The results showed significant differences in the duration of gaze fixation on the human face and the object, as well as in the frequency of gazes. While children with a higher likelihood of ASD exhibited slightly greater pupil dilation compared to NT children, this difference was not statistically significant. Interestingly, the pupil dilation in children with a higher likelihood of ASD remained consistent throughout the task, whereas NT participants showed increased dilation upon hearing the pseudoword.

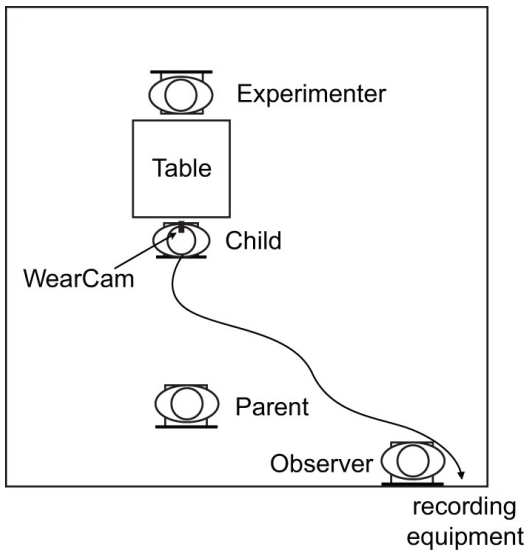

Figure 1: Protocal Setup - Figure from Investigating gaze of children with ASD in naturalistic settings. Noris et. Al

2 Dataset Description

The dataset ("Eye-Tracking Dataset to Support the Research on Autism Spectrum Disorder")[5], published by Federica Cilia et. al, is distributed over 25 CSV-formatted files. Each file represents the output of an eye-tracking experiment. However, a single experiment usually included multiple participants. The participant ID is clearly provided at each record at the 'Participant' column, which can be used to identify the class of participant (i.e., Typically Developing or ASD).

Furthermore, a set of metadata files is included. The main metadata file, Participants.csv, is used to describe the key characteristics of participants (e.g. gender, age, CARS). Every participant was also assigned a unique ID.

3 Preliminary Analysis

In the metadata summary, data was collected from 59 participants, consisting of 38 males and 21 females, with ages ranging from 2.7 to 12.9 years old. Of these participants, 30 were classified as typically developing (TD) and 29 as having Autism Spectrum Disorder (ASD). The mean age of the participants

was 7.88 years, with a standard deviation of 2.79. The CARS (Childhood Autism Rating Scale) scores for the ASD group ranged from 17 to 45, with a mean of 32.97 and a standard deviation of 6.55. These statistics provide a comprehensive overview of the demographics and diagnostic characteristics of the study participants.

ASD Group Statistics:		Neurotypical Group Statistics:		Unidentified(Pos) Group Statistics:	
Eye Position Right X [mm]	**Eye Position Right Y [mm]**	**Eye Position Right X [mm]**	**Eye Position Right Y [mm]**	**Eye Position Right X [mm]**	**Eye Position Right Y [mm]**
count	140735	count	127371	count	8203
140735		127371		8203	
unique	65501	unique	100406	unique	7571
64115		99556		7442	
top	0.0000	top	0	top	0.0000
0.0000		0		0.0000	
freq	24824	freq	8396	freq	231
24824		8396		231	
Eye Position Right Z [mm]	**Eye Position Left X [mm]**	**Eye Position Right Z [mm]**	**Eye Position Left X [mm]**	**Eye Position Right Z [mm]**	**Eye Position Left X [mm]**
count	140735	count	127371	count	8203
134547		111612		8203	
unique	65930	unique	101752	unique	7603
61809		85684		7497	
top	0.0000	top	0	top	0.0000
0.0000		0		0.0000	
freq	24824	freq	8396	freq	231
23095		8367		231	
Eye Position Left Y [mm]	**Eye Position Left Z [mm]**	**Eye Position Left Y [mm]**	**Eye Position Left Z [mm]**	**Eye Position Left Y [mm]**	**Eye Position Left Z [mm]**
count	134547	count	111612	count	8203
134547		111612		8203	
unique	60535	unique	85113	unique	7381
62082		87075		7534	
top	0.0000	top	0	top	0.0000
0.0000		0		0.0000	
freq	23095	freq	8367	freq	231
23095		8367		231	
Pupil Position Right X [px]	**Pupil Position Right Y [px]**	**Pupil Position Right X [px]**	**Pupil Position Right Y [px]**	**Pupil Position Right X [px]**	**Pupil Position Right Y [px]**
count	140735	count	127371	count	
140735		127371		8203	8203
unique	67021	unique	102466	unique	
66511		101704		7462	7423
top	0.0000	top	0	top	
0.0000		0		0.0000	
				0.0000	
freq	26765	freq	9402	freq	
26765		9402		411	411
Pupil Position Left X [px]	**Pupil Position Left Y [px]**	**Pupil Position Left X [px]**	**Pupil Position Left Y [px]**	**Pupil Position Left X [px]**	**Pupil Position Left Y [px]**
count	134547	count	111612	count	8203
134547		111612		8203	
unique	62886	unique	87235	unique	7426
62370		86636		7351	
top	0.0000	top	0	top	0.0000
0.0000		0		0.0000	
freq	24541	freq	9546	freq	508
24541		9546		508	
Point of Regard Right X [px]	**Point of Regard Right Y [px]**	**Point of Regard Right X [px]**	**Point of Regard Right Y [px]**	**Point of Regard Right X [px]**	**Point of Regard Right Y [px]**
count	187817	count	225675	count	
187817		225675		23424	
				23424	
unique	86150	unique	175499	unique	
86388		174032		15343	
				14623	
top	0.0000	top	0.0000	top	
0.0000		0.0000		0.0000	
				0.0000	
freq	50023	freq	15394	freq	
49514		15954		4346	5337
Point of Regard Left X [px]	**Point of Regard Left Y [px]**	**Point of Regard Left X [px]**	**Point of Regard Left Y [px]**	**Point of Regard Left X [px]**	**Point of Regard Left Y [px]**
count	181629	count	209916	count	
181629		209916		23424	23424
unique	81947	unique	160747	unique	
82219		159360		15343	14623
top	0.0000	top	0.0000	top	
0.0000		0.0000		0.0000	
				0.0000	
freq	48032	freq	14909	freq	
47436		15417		4346	5337

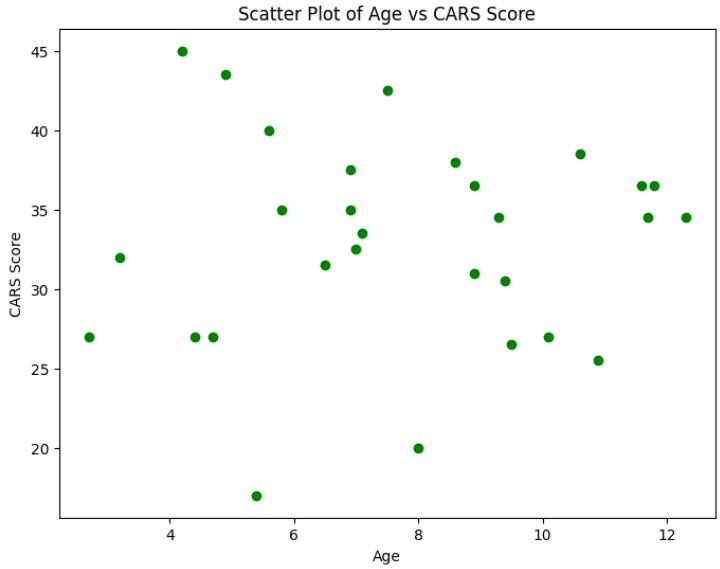

Figure 2: CARS Scatterplot

4 Data Analysis

4.1 Scrubbing Data

To analyze the eye tracking data, the dataset was divided into three subsets based on participant groups. The first subset, asddf (Autism Sprectrum Disorder Dataframe), included data from participants with IDs ranging from 1 to 29, representing individuals with Autism Spectrum Disorder (ASD). The second subset, neurotypicaldf (Neurotypical Dataframe), comprised data from participants with IDs ranging from 30 to 59, representing typically developing (TD) individuals. The third subset, unidentifieddf (Unidentified Dataframe), contained data from participants labeled as 'Unidentified(Pos)', whose group classification was unspecified.

The analysis focused on specific columns related to eye tracking measurements (which will be used as our features for training the model), including 'Eye Position Right X [mm]', 'Eye Position Right Y [mm]', 'Eye Position Right Z [mm]', 'Eye Position Left X [mm]', 'Eye Position Left Y [mm]', 'Eye Position Left Z [mm]', 'Pupil Position Right X [px]', 'Pupil Position Right Y [px]', 'Pupil Position Left X [px]', 'Pupil Position Left Y [px]', 'Point of Regard Right X [px]', 'Point of Regard Right Y [px]', 'Point of Regard Left

Eye Position Right X [mm]: The horizontal position of the right eye in millimeters relative to a reference point.
Eye Position Right Y [mm]: The vertical position of the right eye in millimeters relative to a reference point.
Eye Position Right Z [mm]: The depth position of the right eye in millimeters relative to a reference point.
Eye Position Left X [mm]: The horizontal position of the left eye in millimeters relative to a reference point.
Eye Position Left Y [mm]: The vertical position of the left eye in millimeters relative to a reference point.
Eye Position Left Z [mm]: The depth position of the left eye in millimeters relative to a reference point.
Pupil Position Right X [px]: The horizontal position of the right pupil in pixels relative to a reference point.
Pupil Position Right Y [px]: The vertical position of the right pupil in pixels relative to a reference point.
Pupil Position Left X [px]: The horizontal position of the left pupil in pixels relative to a reference point.
Pupil Position Left Y [px]: The vertical position of the left pupil in pixels relative to a reference point.
Point of Regard Right X [px]: The horizontal point of regard of the right eye in pixels on a display screen.
Point of Regard Right Y [px]: The vertical point of regard of the right eye in pixels on a display screen.
Point of Regard Left X [px]: The horizontal point of regard of the left eye in pixels on a display screen.
Point of Regard Left Y [px]: The vertical point of regard of the left eye in pixels on a display screen.

Figure 3: Feature Selection with Description

X [px]', and 'Point of Regard Left Y [px]'. These columns were deemed crucial for understanding gaze behavior and patterns in individuals with ASD, TD individuals, and those with unspecified classifications, providing valuable insights into the differences in eye tracking metrics across these groups.

Unfortunately, since the gaze vector data was missing in the CSV files (zip file originally downloaded from Kaggle), we are unable to analyze the trajectory of gaze behavior. However, we can still analyze the point of regard, along with pupil position and dilation.

Next, we processed the dataset by converting non-numeric values to NaN (Not a Number) using the pandas pd.tonumeric method. This step ensured that all data was in a consistent format suitable for analysis. Next, I addressed missing values in numerical columns by filling them with the mean of each column using the fillna method.

4.2 Pre-processing Data

In our preprocessing step, we implemented a participant mapping function to categorize individuals based on their participant IDs. The function classified participants into three groups: 'ASD' for IDs 1-29, 'Neurotypical' for IDs 30-59, and 'Other' for participants labeled as 'Unidentified'. We applied this mapping to the 'Participant' column of our DataFrame, creating a new column called 'Participant Group' to store these categories. Then we combine the 3 group dataframes as 'combined dataframe'.

```
X_train shape: (330793, 14), y_train shape: (330793,)
X_val shape: (82699, 14), y_val shape: (82699,)

Mapping of numeric labels to original labels:
Numeric Label: 0, Original Label: 0
Numeric Label: 1, Original Label: 1
Number of classes: 2
```

The output indicates that after preprocessing, we have 349,532 samples in the training set and 87,384 samples in the validation set, each with 14 features. The target labels (y) are correctly shaped, with 349,532 labels for the training set and 87,384 labels for the validation set.

To address class imbalance in the dataset, we use the RandomOverSampler technique. Class imbalance occurs when one class (in this case, 'minority') has significantly fewer samples than another class.

The RandomOverSampler is used to create a balanced dataset by randomly duplicating samples from the minority class until it matches the number of samples in the majority class.

```
Before Class Distribution:
Other           1839451
Neurotypical     225675
ASD              187817
Name: Participant Group, dtype: int64

After Class Distribution:
Balanced Class Distribution (filtering only ASD \& NT):
Class 0: 218024 samples
Class 1: 225675 samples
```

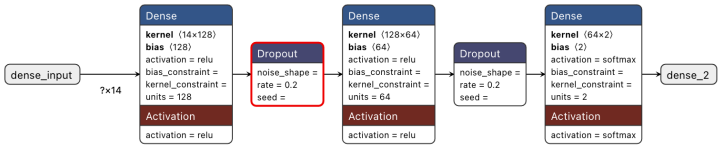

Figure 4: Sequential FNN Model Architecture

4.3 Model Architecture

We have developed two distinct deep learning models for this study. Our choice of implementing a Feedforward Neural Network (FNN) and a Long Short-Term Memory (LSTM) network stems from our belief that these architectures are best suited to leverage the intricacies of our dataset, ensuring optimal performance. The first deep learning model used in this study is a feedforward neural network implemented using the Keras Sequential API with a TensorFlow backend. The model consists of three densely connected layers, including two hidden layers and one output layer. The first hidden layer has 128 units and uses the rectified linear unit (ReLU) activation function. It takes the input shape of the training data, which is 14 features representing various eye tracking measurements.

A dropout layer with a dropout rate of 0.2 is applied after the first hidden layer to reduce overfitting. The second hidden layer has 64 units and also uses the ReLU activation function, followed by another dropout layer with the same dropout rate of 0.2. The output layer consists of 2 units corresponding to the two categories: 'ASD' (Autism Spectrum Disorder) and 'TD' (Typically Developing). It uses the softmax activation function to output the probability distribution over the two classes.

Feedforward Neural Network (FNN) Overview:

Let X be the input vector of size n (number of features).

Let $W^{(1)}$ be the weight matrix of the first hidden layer of size $n \times m$ (number of input features by number of neurons in the hidden layer).

Let $b^{(1)}$ be the bias vector of the first hidden layer of size m (number of neurons in the hidden layer).

Let $H^{(1)}$ be the output vector of the first hidden layer, calculated as

$$H^{(1)} = \text{ReLU}(X \cdot W^{(1)} + b^{(1)})$$

Repeat the process for subsequent hidden layers and the output layer.

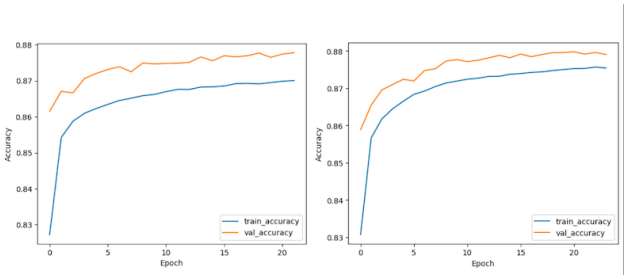

Figure 5: Training Validation Accuracy on FNN (Left) and LSTM (right) models

The final output of the FNN can be represented as

$$Y = \text{Softmax}(H^{(L)} \cdot W^{(L+1)} + b^{(L+1)})$$

, where L is the number of hidden layers, and Softmax is the activation function of the output layer.

The model is compiled using the Adam optimizer with a learning rate of 0.001 and the sparse categorical cross-entropy loss function, suitable for multi-class classification problems. During training, early stopping is applied with a patience of 3 epochs to prevent overfitting and restore the best weights. The model is trained for 50 epochs with a batch size of 32.

In the seventeenth epoch of training, the model achieved a loss of 0.2919 and an accuracy of 87.09 on the training data. During this epoch, the validation accuracy was 87.62. The training process was performed on a dataset comprising 10338 samples, with each iteration taking approximately 36 seconds. The validation loss and accuracy were 0.2779 and 87.62, respectively, indicating good performance and generalization of the model on unseen data. The training has stopped on the seventeeth epoch.

The second deep learning model utilized in this study is an LSTM (Long Short-Term Memory) neural network, implemented using the Keras Sequential API with a TensorFlow backend. The model architecture includes an LSTM layer with 128 units and a rectified linear unit (ReLU) activation function, designed to process sequential data. The input shape is specified as (1, Xtrain.shape[2]), indicating that the model expects input sequences with a length of 1 and a feature dimension matching the number of features in the training data (14 in this case).

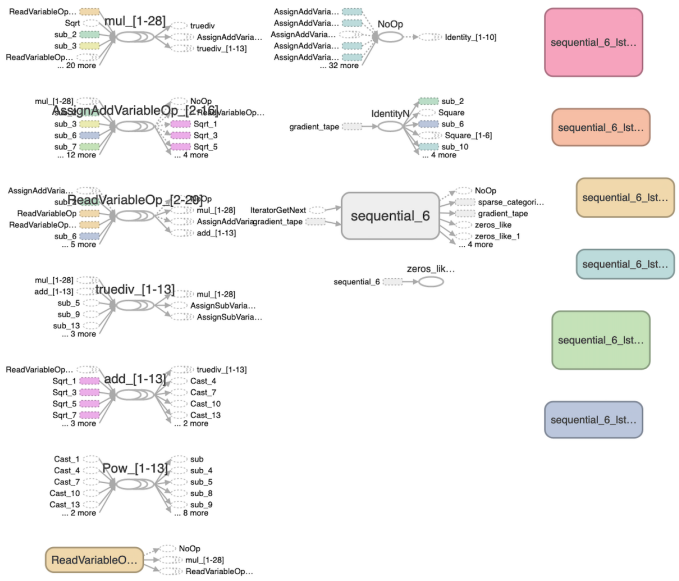

Figure 6: LSTM Graph Architecture

Spatial data of eye tracking measurements represents non-image data that contains sequential information over time. For such data, an LSTM is particularly useful due to its ability to capture dependencies and patterns over time. Unlike a Sequential feedforward neural network, which processes each input independently, an LSTM maintains an internal state that allows it to remember information from previous time steps. This makes it well-suited for tasks involving temporal sequences, such as analyzing eye tracking data collected over multiple time points during an experiment or task.

The key mechanism behind an LSTM is its ability to selectively retain or forget information over time through specialized units called memory cells. Each memory cell has three main components: an input gate, a forget gate, and an output gate. These gates regulate the flow of information into, out of, and within the memory cell, allowing the LSTM to selectively update its internal state based on the input data and its own previous state. This enables the LSTM to learn long-term dependencies in the input sequence while mitigating the vanishing gradient problem commonly encountered in traditional RNNs.

To prevent overfitting, a dropout layer with a dropout rate of 0.2 is applied after the LSTM layer. The model then includes a dense hidden layer with

64 units and a ReLU activation function, followed by another dropout layer with the same dropout rate.

The output layer consists of 2 units, representing the two categories: 'ASD' (Autism Spectrum Disorder) and 'TD' (Typically Developing). The softmax activation function is used in the output layer to compute the probability distribution over the two classes. The model is compiled using the Adam optimizer with a learning rate of 0.001 and the sparse categorical cross-entropy loss function, suitable for multi-class classification problems. Early stopping is applied during training with a patience of 3 epochs, restoring the best weights based on validation performance to prevent overfitting.

Overview of Long Short-Term Memory (LSTM):
Let X_t be the input at time step t.
Let h_t be the hidden state at time step t.
Let c_t be the cell state at time step t.
The LSTM equations can be represented as follows:

$$
\begin{aligned}
f_t &= \sigma(W_f \cdot [h_{t-1}, X_t] + b_f) \\
i_t &= \sigma(W_i \cdot [h_{t-1}, X_t] + b_i) \\
o_t &= \sigma(W_o \cdot [h_{t-1}, X_t] + b_o) \\
\tilde{c}_t &= \tanh(W_c \cdot [h_{t-1}, X_t] + b_c) \\
c_t &= f_t \odot c_{t-1} + i_t \odot \tilde{c}_t \\
h_t &= o_t \odot \tanh(c_t)
\end{aligned}
$$

where σ is the sigmoid activation function, $\odot$ denotes element-wise multiplication, and $[\cdot, \cdot]$ denotes concatenation.

The LSTM model is trained for 50 epochs with a batch size of 32, optimizing its ability to learn sequential patterns from the eye tracking measurements provided in the training data.

4.3.1 Predictions

The Sequential FNN model's predictions were applied to the entire training dataset consisting of 10,338 samples, categorizing each sample as either 'Neurotypical' or 'ASD'. The resulting training data accuracy, approximately 87.58, signifies the proportion of correct predictions compared to the actual labels. Similarly, for the validation dataset comprising 2,585 samples, the

Classifiers		Performance Metrics (%):			
Sequential Model		**precision**	**recall**	**f1-score**	**support**
	ASD	0.87	0.86	0.86	37514
	Neurotypical	0.88	0.89	0.89	45185
	accuracy			0.88	82699
	macro avg	0.88	0.87	0.87	82699
	weighted avg	0.88	0.88	0.88	82699
			AUC: 0.0509. **Probability of ASD Class		
Long Short Term Memory (LSTM) Model	ASD	0.87	0.86	0.87	37514
	Neurotypical	0.88	0.90	0.89	45185
	accuracy			0.88	82699
	macro avg	0.88	0.88	0.88	82699
	weighted avg	0.88	0.88	0.88	82699
			AUC: 0.0478. **Probability of ASD Class		

Figure 7: Performance Metrics of Sequential FNN & LSTM

model's predictions were compared to the true labels, yielding a validation data accuracy of approximately

87.63. These results demonstrate the model's ability to make predictions for both training and validation datasets, indicating its effectiveness in classifying individuals as 'Neurotypical' or 'ASD'. Based on the performance metrics of the Sequential Model and the Long Short-Term Memory (LSTM) Model, it can be concluded that both models achieve comparable results in classifying individuals as 'ASD' (Autism Spectrum Disorder) or 'Neurotypical'. Both models demonstrate high precision, recall, and F1-scores for the 'ASD' class, indicating that they are effective at correctly identifying individuals with ASD. However, the AUC values for both models suggest that they perform only slightly better than random chance in distinguishing between 'ASD' and 'Neurotypical' samples based on the probability of the 'ASD' class. These findings suggest that while the models are effective at identifying individuals with ASD based on the features extracted from eye tracking measurements, further refinement may be needed to improve their ability to distinguish between 'ASD' and 'Neurotypical' individuals.

4.4 Analyzing Pupil Features

We created a correlation matrix which would give us insight into the relationships between different features in the dataset after scaling. Each value in

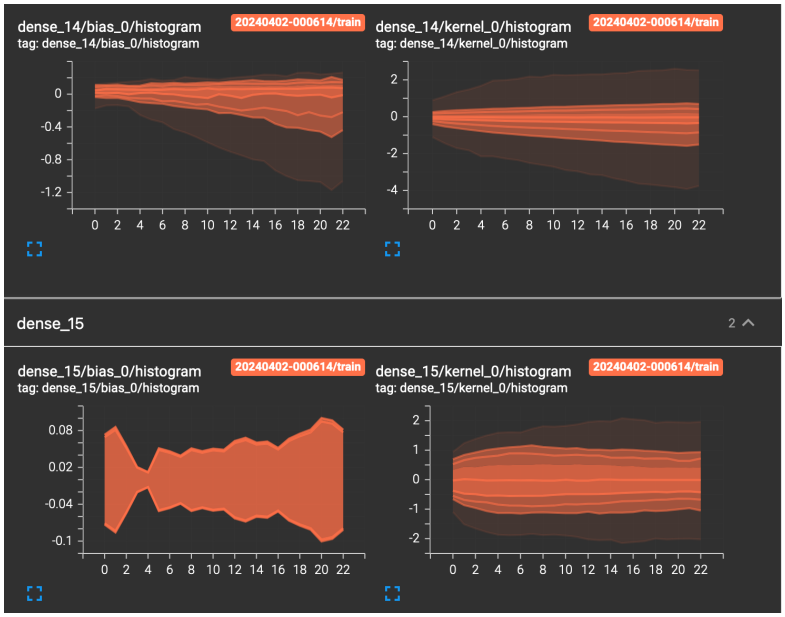

Figure 8: LSTM Training Distribution

the matrix represents the correlation coefficient between two features, ranging from -1 to 1.

For example, a correlation coefficient of approximately 0.94 between 'Eye Position Left Y [mm]' and 'Eye Position Left Z [mm]' suggests a strong positive correlation, indicating that these two features tend to increase or decrease together. Conversely, a correlation coefficient of approximately -0.66 between 'Eye Position Right Y [mm]' and 'Point of Regard Left X [px]' indicates a moderate negative correlation, suggesting that as one feature increases, the other tends to decrease.

4.4.1 ANOVA Test & Spearman's Correlation

The ANOVA tests conducted on various eye tracking measurements for participants with Autism Spectrum Disorder (ASD), Neurotypical individuals, and participants labeled as Unidentified(Pos) which revealed statistically significant differences in several key metrics. For 'Eye Position Left X [mm]', 'Eye Position Left Y [mm]', 'Eye Position Left Z [mm]', 'Pupil Position Left X [px]', 'Pupil Position Left Y [px]', 'Point of Regard Left X [px]', and 'Point of Regard Left Y [px]', the F-statistics were 18134.17, 13128.42, 12140.71,

9476.12, 880.72, 16103.98, and 13048.19, respectively, all with p-values below 0.001. These results suggest highly significant differences in these measurements between the three participant groups.


Violin plot of Eye Position Right X [mm] by Participant Group
Eye Position Right X [mm]
150
100
50
0
−50
−100
−150
−200
ASD
Neurotypical
Participant Group


Violin plot of Eye Position Right Y [mm] by Participant Group
Eye Position Right Y [mm]
100
50
0
−50
−100
−150
ASD
Neurotypical
Participant Group

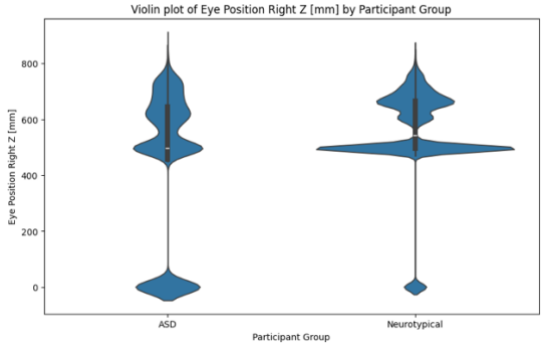
Violin plot of Eye Position Right Z [mm] by Participant Group
Eye Position Right Z [mm]
800
600
400
200
0
ASD
Neurotypical
Participant Group

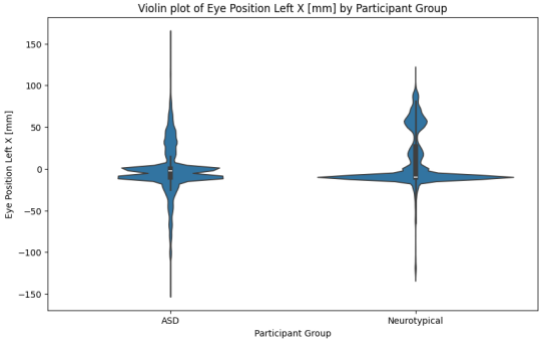
Violin plot of Eye Position Left X [mm] by Participant Group
Eye Position Left X [mm]
150
100
50
0
−50
−100
−150
ASD
Neurotypical
Participant Group

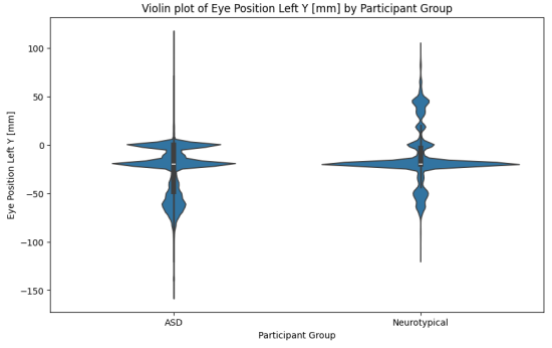
Violin plot of Eye Position Left Y [mm] by Participant Group
Eye Position Left Y [mm]
100
50
0
−50
−100
−150
ASD
Neurotypical
Participant Group

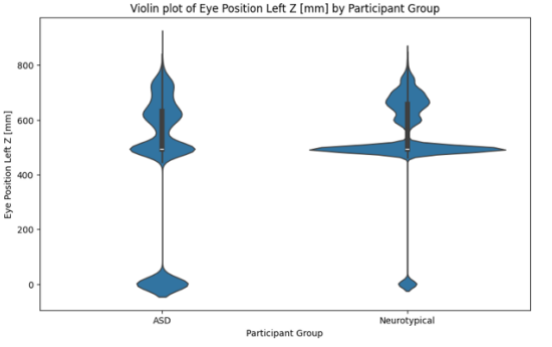
Violin plot of Eye Position Left Z [mm] by Participant Group
Eye Position Left Z [mm]
800
600
400
200
0
ASD
Neurotypical
Participant Group

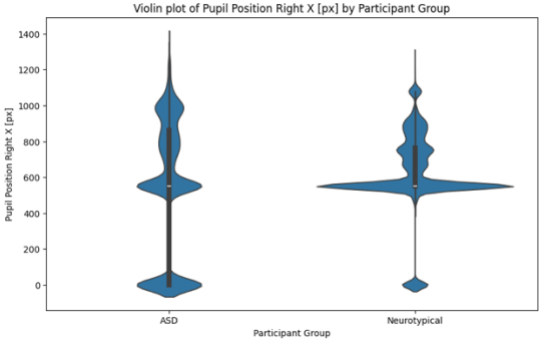
Violin plot of Pupil Position Right X [px] by Participant Group
Pupil Position Right X [px]
1400
1200
1000
800
600
400
200
0
ASD
Neurotypical
Participant Group

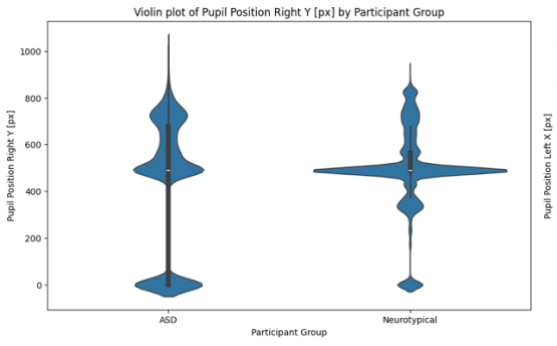
Violin plot of Pupil Position Right Y [px] by Participant Group
Pupil Position Right Y [px]
1000
800
600
400
200
0
ASD
Neurotypical
Participant Group

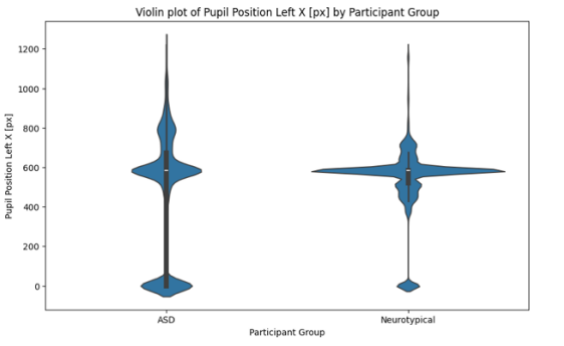
Violin plot of Pupil Position Left X [px] by Participant Group
Pupil Position Left X [px]
1200
1000
800
600
400
200
0
ASD
Neurotypical
Participant Group

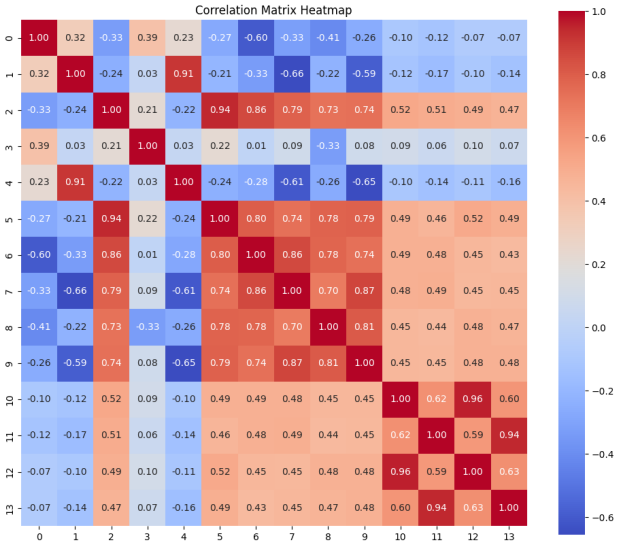

Figure 9: Correlation Matrix of Relationship of Eye Features

The correlation analysis reveals interesting insights into the relationship between different eye tracking metrics. In the ASD group, strong negative correlations were observed between eye position and pupil position, with coefficients ranging from -0.776 to -0.358. This suggests that as the eye position on the left increases, the left pupil position tends to decrease significantly. In contrast, the neurotypical group displayed weaker correlations, with coefficients ranging from -0.657 to -0.412, indicating a less pronounced relationship between these variables. The unidentified group showed similar patterns to the ASD group, with coefficients ranging from -0.816 to -0.044.

These findings provide valuable insights into the interplay between different eye tracking metrics and can inform future research on eye movement patterns and their underlying mechanisms.

5 Limitations

While the ANOVA results provide valuable insights into the differences in eye tracking measurements among individuals with Autism Spectrum Disorder (ASD), Neurotypical individuals, and those in the Unidentified(Pos) group, there are several limitations to consider. Firstly, the sample sizes

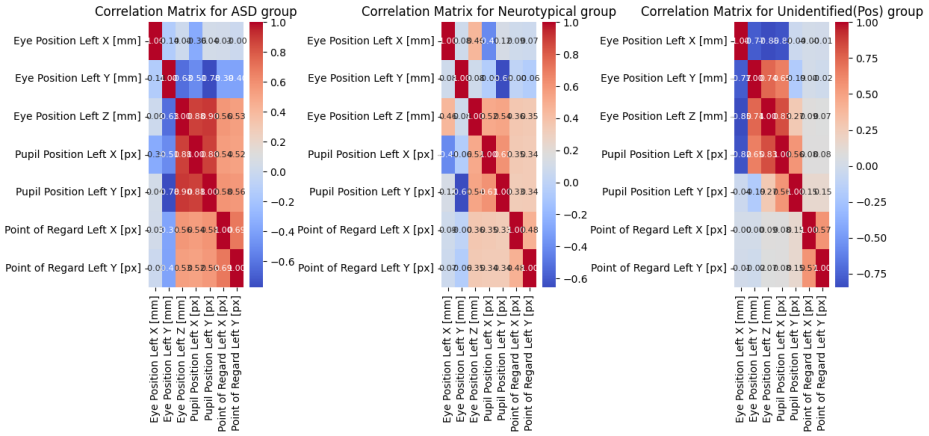

Figure 10: Correlation Matrix of ASD, NT, and UNI

for each group may affect the generalizability of the findings, especially for the Unidentified(Pos) group, which might be relatively small compared to the ASD and Neurotypical groups. Additionally, the study's cross-sectional nature limits the ability to establish causal relationships between the eye tracking measurements and the participants' conditions. Furthermore, the use of ANOVA does not account for potential confounding variables that could influence the results. Future research could benefit from larger and more diverse samples, longitudinal designs, and multivariate analyses to better understand the complexities of eye tracking data in the context of autism spectrum disorders.

There are several limitations that should be considered when interpreting the correlational results as well. First, there may be sample bias if certain groups are not adequately represented, impacting the generalizability of the findings. Measurement errors, such as inaccuracies in data collection or entry, could introduce noise and affect the accuracy of the correlation estimates. The dataset that was download had missing data in every CSV file. It was unfortuante that

6 Concluding Thoughts

In conclusion, our project demonstrates the effectiveness of both the Sequential Feedforward Neural Network (FNN) model and the Long Short-Term

Memory (LSTM) model in classifying individuals as 'ASD' (Autism Spectrum Disorder) or 'Neurotypical' based on eye tracking measurements. The Sequential FNN model achieved high accuracy for both the training and validation datasets, indicating its ability to generalize well to unseen data. Additionally, the ANOVA tests conducted on various eye tracking measurements revealed significant differences between individuals with ASD, neurotypical individuals, and those labeled as Unidentified(Pos). These findings highlight the potential of eye tracking metrics as biomarkers for ASD diagnosis. Furthermore, the correlation analysis provided insights into the relationship between different eye tracking metrics, with strong negative correlations observed in the ASD group compared to weaker correlations in the neurotypical group. Our project aims to inspire further research into understanding the nature of eye behavior in Autism Spectrum Disorder (ASD) through the application of machine learning models and analysis of eye tracking data. We emphasize the importance of ongoing exploration in this field to advance our understanding.

7 Bibliography

1. Chiarotti, F.; Venerosi, A. Epidemiology of Autism Spectrum Disorders: A Review of Worldwide Prevalence Estimates Since 2014. Brain Sci. 2020, 10, 274. [Google Scholar] [CrossRef] [PubMed]

2. Guha, M. Diagnostic and Statistical Manual of Mental Disorders: DSM-5; American Psychiatric Association: Washington, DC, USA, 2013. [Google Scholar]

3. Noris, B., Barker, M., Nadel, J., Hentsch, F., Ansermet, F., & Billard, A. (2011). Measuring gaze of children with autism spectrum disorders in naturalistic interactions. In Engineering in Medicine and Biology Society, EMBC, 2011 Annual International Conference of the IEEE (pp. 5356–5359).

4. Camero R, Martínez V, Gallego C. Gaze Following and Pupil Dilation as Early Diagnostic Markers of Autism in Toddlers. Children (Basel). 2021 Feb 5;8(2):113. doi: 10.3390/children8020113. PMID: 33562656; PMCID: PMC7914719.

   Dataset Citation:

5. Cilia, F., Carette, R., Elbattah, M., Guérin, J., & Dequen, G. (2022). Eye-Tracking Dataset to Support the Research on Autism Spectrum Disorder. In Proceedings of the IJCAI–ECAI Workshop on Scarce Data in Artificial Intelligence for Healthcare (SDAIH).